Spin reorientation and metamagnetic transitions in $R\mathrm{Fe}_{0.5}\mathrm{Cr}_{0.5}\mathrm{O}_3$ perovskites (R = Tb, Dy, Ho, Er)

Juan P. Bolletta,[1] Fernando Pomiro,[2] Rodolfo D. Sánchez,[3,4] Vladimir Pomjakushin,[5] Gabriela Aurelio,[3] Antoine Maignan,[6] Christine Martin,[6] and Raúl E. Carbonio[1,*]

[1]*INFIQC (Consejo Nacional de Investigaciones Científicas y Técnicas [CONICET]–Universidad Nacional de Córdoba), Departamento de Fisicoquímica, Facultad de Ciencias Químicas, Universidad Nacional de Córdoba, Haya de la Torre Esq. Medina Allende, Ciudad Universitaria, X5000HUA Córdoba, Argentina*

[2]*Instituto de Física del Litoral (CONICET-Universidad Nacional del Litoral), Güemes 3450, S3000GLN Santa Fe, Argentina*

[3]*Centro Atómico Bariloche, Comisión Nacional de Energía Atómica, CONICET, 8400 San Carlos de Bariloche (RN), Argentina*

[4]*Instituto Balseiro, Universidad Nacional de Cuyo, 8400 San Carlos de Bariloche (RN), Argentina*

[5]*Laboratory for Neutron Scattering and Imaging (LNS), Paul Scherrer Institute, Villigen CH-5232, Switzerland*

[6]*Laboratoire CRISMAT, UMR 6508 Centre National de la Recherche Scientifique (CNRS)/ENSICAEN/Université de Caen Normandie (UNICAEN), 6 Boulevard Marechal Juin, 14050 Caen cedex, France*

(Received 21 June 2018; revised manuscript received 29 August 2018; published 10 October 2018)

In this work we present the magnetic structures and spin reorientation (SR) transitions of the mixed orthochromite-orthoferrite perovskites $R\mathrm{Fe}_{0.5}\mathrm{Cr}_{0.5}\mathrm{O}_3$ (R = Tb, Dy, Ho, Er). Magnetization as a function of temperature and external magnetic field as well as neutron powder diffraction measurements were used to characterize the magnetic transitions, including the SR transitions in the transition metal sublattice and the ordering of the rare earth sublattice. The studied compounds order antiferromagnetically below 270 K in a $\mathbf{G_x}$ configuration compatible with the Γ_4 representation. As temperature decreases, all the compounds show a SR transition from $\mathbf{G_x}$ (Γ_4) to $\mathbf{G_z}$ (Γ_2). This transition occurs in a wide temperature range, where both magnetic configurations coexist. Below this SR, the behavior in each case depends on the rare earth. $\mathrm{HoFe}_{0.5}\mathrm{Cr}_{0.5}\mathrm{O}_3$ shows Ho^{3+} sublattice ordering at a relatively high temperature (45 K). $\mathrm{DyFe}_{0.5}\mathrm{Cr}_{0.5}\mathrm{O}_3$ and $\mathrm{ErFe}_{0.5}\mathrm{Cr}_{0.5}\mathrm{O}_3$ show a second SR transition of the transition metal sublattice, from $\mathbf{G_z}$ (Γ_2) to $\mathbf{G_y}$ (Γ_1) at low temperatures (15 and 8 K, respectively). Below these temperatures a metamagnetic (MM) transition is observed for these two compounds at an external magnetic field of $H \approx 7$ kOe. The fact that this is only observed for compounds showing $\mathbf{G_z}$ (Γ_2) to $\mathbf{G_y}$ (Γ_1) transition suggests that there is a correlation between the $\mathbf{G_y}$ (Γ_1) order and the MM transition. Finally, $\mathrm{TbFe}_{0.5}\mathrm{Cr}_{0.5}\mathrm{O}_3$ is a peculiar case, since it is the only compound in this family that shows a re-entrant SR to $\mathbf{G_x}$ (Γ_4) at very low temperatures. By combining these results with previous reports on $R\mathrm{FeO}_3$, $R\mathrm{CrO}_3$, and $R\mathrm{Fe}_{0.5}\mathrm{Cr}_{0.5}\mathrm{O}_3$, we develop a method to qualitatively estimate the SR temperature and the type of transition. We also propose a complete magnetic phase diagram containing the SR transitions and R^{3+} ordering temperatures for all the $R\mathrm{Fe}_{0.5}\mathrm{Cr}_{0.5}\mathrm{O}_3$ (R = Tb, Dy, Ho, Er, Tm, Yb, and Lu) compounds.

DOI: 10.1103/PhysRevB.98.134417

I. INTRODUCTION

Materials with the ABO_3 perovskite structure have been regarded for a long time as a playground for solid state chemistry because of the wide extent of properties that can be achieved within them. This is due to their enormous flexibility in composition, the different types of order that might arise in its sublattices, and also to the possibility of displaying vacancies and nonstoichiometry, among other reasons. A particular group of perovskites $R\mathrm{MO}_3$, with rare earth cations (R^{3+}) in the A site and first-row transition metal cations (M^{3+}) in the B site has been thoroughly investigated for more than 50 years. Many of their interesting properties arise from the complex magnetic interactions between cations containing unpaired $3d$ and $4f$ electrons. Two particular families have been extensively studied: orthochromites ($R\mathrm{CrO}_3$) and orthoferrites ($R\mathrm{FeO}_3$). The Cr^{3+} sublattice in orthochromites usually orders antiferromagnetically between 120 and 300 K, while in orthoferrites the Fe^{3+} sublattice also orders antiferromagnetically but at higher temperatures, between 620 and 740 K. In both cases, the temperature of this transition depends on the rare earth [1,2]. The notorious difference in the ordering temperature between these two families is attributed to the Fe^{3+}-O^{2-}-Fe^{3+} superexchange interactions being much stronger than Cr^{3+}-O^{2-}-Cr^{3+} superexchange interactions. Although the ordering is mainly antiferromagnetic, it allows a small canting that produces a net weak ferromagnetic moment [3,4]. In some cases, magnetic order is also observed in the rare earth sublattice. This occurs at much lower temperatures, usually below 10 K. Above this temperature, R^{3+} cations behave paramagnetically [1,2].

Among the properties of these compounds, we focus on the presence of spin reorientation (SR) transitions, which consist of a rotation of the magnetic moments with respect to a crystallographic axis. The SR transition can be triggered by a temperature change, an external magnetic field [5], or even by a laser pulse [6]. The SR transition is caused

*Corresponding author: carbonio@fcq.unc.edu.ar

by both anisotropic-symmetric exchange and antisymmetric Dzyaloshinskii-Moriya (DM) interactions between M^{3+} and R^{3+}. The temperatures at which this type of transition occurs as well as the magnetic structures before and after SR are all conditioned by the combination of cations and their magnetic interactions [7]. SR has also been reported in $YFe_{1-x}Mn_xO_3$, which contains a nonmagnetic ion in the A site and two different transition metal cations randomly distributed in the B site. In this case, SR is thought to be caused by the different magnetic anisotropy contribution of each transition metal cation [8].

Various other striking properties have been observed in related orthochromites and orthoferrites including magnetocaloric effects [9–12], magnetization reversal [13,14], negative thermal expansion [14], and diverse magnetoelectric effects [11,15–17]. All these properties are highly dependent on magnetic interactions between the involved cations [18]. Another interesting observation is the appearance of ferroelectricity in connection with the weak ferromagnetism of the transition metal sublattice, since polarization disappears when the perovskites undergo a SR transition onto a magnetic structure with no canting [19–22]. It is clear that different mixtures of cations add further complexity to the system which can lead to new properties. Furthermore, a deep knowledge of the relevant interactions allows tuning of these properties and the temperature at which they occur by modifying the stoichiometry of the designed compound [17,23–25].

In this context we explore the magnetic structures and SR transitions of the mixed orthochromite-orthoferrite $RFe_{0.5}Cr_{0.5}O_3$ perovskites (R = Tb, Dy, Ho, and Er) by means of neutron powder diffraction (NPD) and magnetization measurements. Combining our data with a recent report on the related $RFe_{0.5}Cr_{0.5}O_3$ (R = Tm, Yb, and Lu) system [14], we propose a complete magnetic phase diagram containing all the SR transitions and R^{3+} ordering temperatures for all the compounds $RFe_{0.5}Cr_{0.5}O_3$ (R = Tb, Dy, Ho, Er, Tm, Yb, and Lu).

II. EXPERIMENTAL DETAILS

$RFe_{0.5}Cr_{0.5}O_3$ (R = Tb, Dy, Ho, and Er) samples were prepared in polycrystalline form via a precursor obtained by a wet chemical route. Stoichiometric amounts of R_2O_3 (99.9+%, STREM), $Fe(NO_3)_3 \cdot 9H_2O$ (analytical grade, Merck) and $Cr(NO_3)_3 \cdot 9H_2O$ (99.9+%, STREM) were dissolved in a mixture of nitric and citric acid. By producing a reactive precursor from a solution, a random distribution of cations was facilitated. The citrate solution was slowly evaporated, leading to a gel, which then turned into dry flakes with further evaporation. This product was dried and then decomposed at 600 °C in air for 12 h. The resulting precursor was ground, pressed into pellets, and treated at 1050 °C in air for 12 h. The final product is a brown-orange powder.

Neutron powder diffraction (NPD) patterns were obtained from experiments carried out in the HRPT instrument at the SINQ facility in the Paul Scherrer Institut (PSI), Villigen, Switzerland. Patterns were collected at various temperatures for each sample, with $\lambda = 1.8857$ Å in the 3.55° to 164.5° 2θ range with a 0.05° step. With the obtained data, the refinement of crystal and magnetic structures was performed by means of the Rietveld method [26] with the FULLPROF program [27]. To aid in the determination of magnetic structures, the program BasIReps was used to generate possible candidates for symmetry analysis.

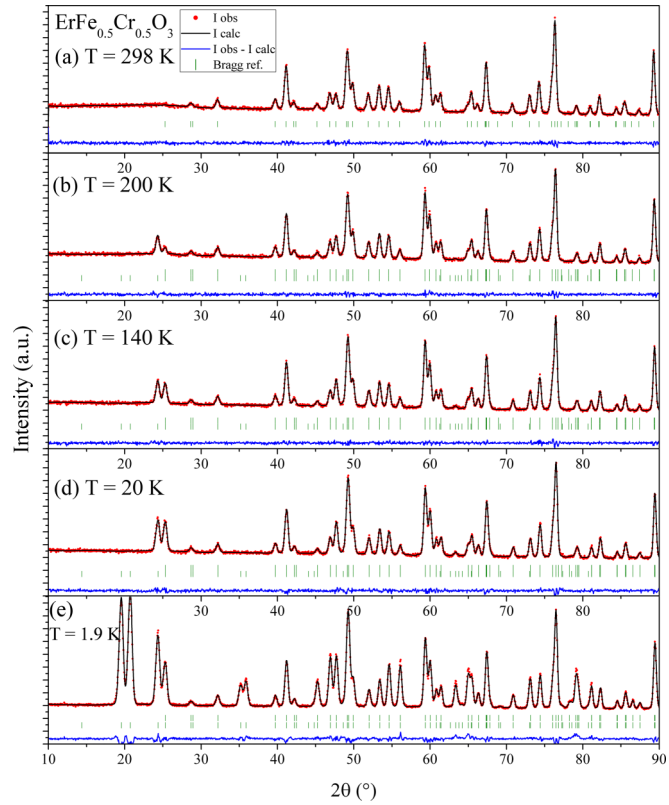

FIG. 1. Observed (red circles) and calculated (black line) NPD patterns at different temperatures with $\lambda = 1.8857$ Å for the $ErFe_{0.5}Cr_{0.5}O_3$ sample. Vertical marks below the patterns indicate Bragg reflections (upper: nuclear; lower: magnetic). Difference pattern plotted at the bottom (blue line).

Magnetic measurements were performed using a commercial MPMS-5S superconducting quantum interference device magnetometer on powdered samples in capsules, warming from 5 to 400 K at 100 Oe in zero-field-cooled and field-cooled (ZFC-FC) modes. Isothermal magnetization loops were performed from −5 to +5 T at 5 K. For erbium and dysprosium samples, additional isothermal magnetization measurements were performed in the 0 to +5 T range at selected temperatures.

III. RESULTS AND DISCUSSION

A. Crystallographic characterization and symmetry considerations

From room temperature NPD data of the $RFe_{0.5}Cr_{0.5}O_3$ perovskites, a distorted perovskite structure belonging to the orthorhombic *Pbnm* space group was refined in all cases. Figure 1 shows five representative NPD patterns obtained at different temperatures for $ErFe_{0.5}Cr_{0.5}O_3$ and their corresponding calculated patterns. Table I summarizes the refined cell parameters at 298 K. The refined structure contains four unit formulas per unit cell and is shown in Fig. 2(a). Table SM-I

TABLE I. Refined cell parameters and cell volume from NPD data at room temperature for $R\mathrm{Fe}_{0.5}\mathrm{Cr}_{0.5}\mathrm{O}_3$. R^{3+} size decreases from left to right, which is reflected in the refined parameters. Space group is *Pbnm*.

	$\mathrm{TbFe}_{0.5}\mathrm{Cr}_{0.5}\mathrm{O}_3$	$\mathrm{DyFe}_{0.5}\mathrm{Cr}_{0.5}\mathrm{O}_3$	$\mathrm{HoFe}_{0.5}\mathrm{Cr}_{0.5}\mathrm{O}_3$	$\mathrm{ErFe}_{0.5}\mathrm{Cr}_{0.5}\mathrm{O}_3$
a (Å)	5.31334(3)	5.28895(5)	5.26562(4)	5.24501(3)
b (Å)	5.56029(4)	5.56140(6)	5.55746(4)	5.55222(3)
c (Å)	7.61125(6)	7.59252(7)	7.57493(5)	7.55682(4)
V (Å^3)	224.864(3)	223.326(4)	221.669(3)	220.065(2)

in the Supplemental Material [29] presents the refined atomic positions, isotropic temperature factors, and occupancies. R^{3+} cations occupy 4*c* (x, y, 1/4) sites. Fe^{3+} and Cr^{3+} cations are randomly distributed in the 4*b* (1/2, 0, 0) sites and are octahedrally coordinated by O^{2-} anions, which occupy two different Wyckoff positions: 4*c* (x, y, 1/4) sites and 8*d* (x, y, z) sites. For future convenience, transition metal and rare earth cations inside the *Pbnm* unit cell are numbered as follows:

$$\begin{aligned} 4b\ \text{site}(\mathrm{Fe}^{3+}/\mathrm{Cr}^{3+}) : n = {} & 1(1/2, 0, 0); 2(1/2, 0, 1/2); \\ & 3(0, 1/2, 1/2); 4(0, 1/2, 0)\ \text{and} \\ 4c\ \text{site}(R^{3+}) : n = {} & 1(x, y, 1/4); 2(-x, -y, -1/4); \\ & 3(x + 1/2, -y + 1/2, -1/4); \\ & 4(-x + 1/2, y + 1/2, 1/4). \end{aligned}$$

For symmetry analysis and interpretation of magnetic structures, the formalism of representation theory, as summarized by Bertaut [30], was used. This method is based on the use of irreducible representations of the crystallographic space groups to investigate the symmetry transformation properties of magnetic structures.

We call S_{nt} the magnetic moment component of ion n along the t direction. Four basis vectors are proposed as a means to decompose a three-dimensional magnetic structure. For example, for the x direction:

$$\begin{aligned} \mathbf{F_x} &= S_{1x} + S_{2x} + S_{3x} + S_{4x}, \\ \mathbf{A_x} &= S_{1x} - S_{2x} - S_{3x} + S_{4x}, \\ \mathbf{G_x} &= S_{1x} - S_{2x} + S_{3x} - S_{4x}, \\ \mathbf{C_x} &= S_{1x} + S_{2x} - S_{3x} - S_{4x}. \end{aligned}$$

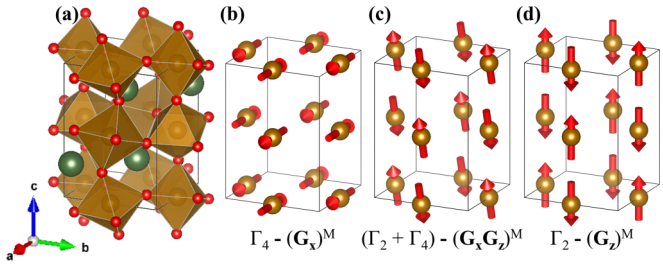

FIG. 2. (a) Drawing of a typical $R\mathrm{MO}_3$ orthorhombic perovskite. R^{3+} in green, M^{3+} in brown, presenting octahedral coordination by O^{2-} in red. (b)–(d) Schematics of the SR transition on the transition metal sublattice, from $\mathbf{G_x}$ to $\mathbf{G_z}$. Magnetic moments are multiplied by a factor of 1.88 in (b) and 1.18 in (c) for clarity. All structural drawings in this article were elaborated with the VESTA software [28].

The **F** basis vector corresponds to a ferromagnetic order, while the others represent three types of antiferromagnetic orders. The eight irreducible representations for the *Pbnm* space group when the propagation vector is $\mathbf{k} = (0, 0, 0)$ can now be expressed as a function of basis vectors in each direction. These are summarized in Table II. Each irreducible representation produces a magnetic structure defined within one Shubnikov magnetic space group, also included in Table II. A magnetic structure displaying combinations of irreducible representations will lead to a lower-symmetry space group, i.e., the magnetic space group resulting from the intersection of the magnetic space groups associated with each involved irreducible representation. This "general group" may be monoclinic or even triclinic, which can be of special interest when considering magnetoelectric couplings, noncentrosymmetric polar structures, and symmetry-based properties in general.

B. Magnetization measurements and $\mathbf{G_x}$-$\mathbf{G_z}$ spin reorientation transition

ZFC and FC dc magnetic susceptibility curves as a function of temperature under an applied field of 100 Oe are shown in Fig. 3. Even if the temperature evolution of the magnetization is highly dependent on the rare earth, the curves do share some similarities. The main shared feature is the onset of the splitting of ZFC and FC curves around 270 K. This is related to the antiferromagnetic ordering of the Fe^{3+}/Cr^{3+} sublattice. Another similarity between these samples is a change in slope of the magnetization curve, usually in the 120–200 K range, which we relate to the first SR as we will show later. Below this temperature all samples except $\mathrm{HoFe}_{0.5}\mathrm{Cr}_{0.5}\mathrm{O}_3$ exhibit an increase in magnetization, leading to a maximum followed by an abrupt drop. These drops are related to SR and magnetic ordering of the

TABLE II. Irreducible representations for *Pbnm* space group when $\mathbf{k} = (0, 0, 0)$ in terms of **F**, **C**, **G**, and **A** basis functions for each site, together with the Shubnikov magnetic space group where the possible resultant magnetic structures are defined [30].

	4*b* site (Fe^{3+}/Cr^{3+})	4*c* site (R^{3+})	Magnetic group
Γ_1	$\mathbf{A_x\,G_y\,C_z}$	$\cdot\cdot\,\mathbf{C_z}$	*Pbnm*
Γ_2	$\mathbf{F_xC_yG_z}$	$\mathbf{F_xC_y}\cdot$	*Pbn'm'*
Γ_3	$\mathbf{C_xF_yA_z}$	$\mathbf{C_xF_y}\cdot$	*Pb'nm'*
Γ_4	$\mathbf{G_x\,A_yF_z}$	$\cdot\cdot\,\mathbf{F_z}$	*Pb'n'm*
Γ_5	···	$\mathbf{G_x\,A_y}\cdot$	*Pb'n'm'*
Γ_6	···	$\cdot\cdot\,\mathbf{A_z}$	*Pb'nm*
Γ_7	···	$\cdot\cdot\,\mathbf{G_z}$	*Pbn'm*
Γ_8	···	$\mathbf{A_xG_y}\cdot$	*Pbnm'*

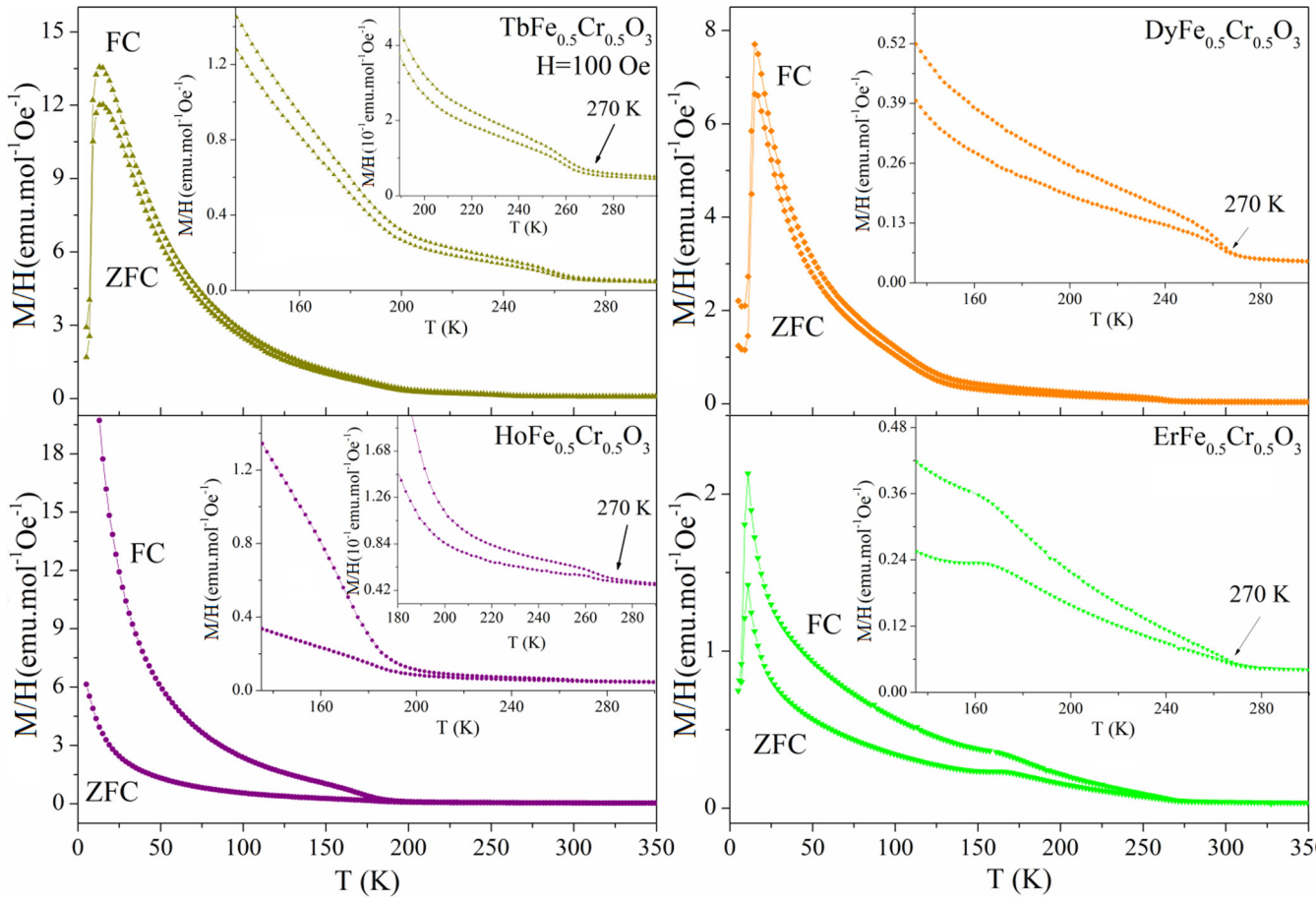

FIG. 3. Magnetization curves for $R\mathrm{Fe}_{0.5}\mathrm{Cr}_{0.5}\mathrm{O}_3$ (R = Tb, Dy, Ho, and Er) as a function of temperature measured at 100 Oe. Insets highlight the magnetic transition at 270 K.

R^{3+} sublattice, as shown below. $\mathrm{HoFe}_{0.5}\mathrm{Cr}_{0.5}\mathrm{O}_3$ does not display a magnetization drop but it does show ordering in the Ho^{3+} sublattice at low temperatures.

Isothermal magnetization measurements as a function of applied field are shown in Fig. 4. The nonlinear responses observed at 5 K are understood as a combination of the canted antiferromagnetic order of the $\mathrm{Fe}^{3+}/\mathrm{Cr}^{3+}$ sublattice combined with the R^{3+} paramagnetic behavior. This is similar to the observations performed in $\mathrm{TmFe}_{0.5}\mathrm{Cr}_{0.5}\mathrm{O}_3$ [14]. Again, the exception is $\mathrm{HoFe}_{0.5}\mathrm{Cr}_{0.5}\mathrm{O}_3$, displaying a loop consistent with ferromagnetic behavior. $\mathrm{ErFe}_{0.5}\mathrm{Cr}_{0.5}\mathrm{O}_3$ and $\mathrm{DyFe}_{0.5}\mathrm{Cr}_{0.5}\mathrm{O}_3$ show a metamagnetic (MM) transition at approximately 7 kOe. Additional isothermal magnetization measurements were performed to assess the nature of these transitions. The specific results of these experiments are analyzed later in this article.

In agreement with the magnetic behavior, all these $R\mathrm{Fe}_{0.5}\mathrm{Cr}_{0.5}\mathrm{O}_3$ perovskites also share similarities in their magnetic structures. These structures were obtained from the analysis of the NPD data. As an example, five NPD patterns measured at different temperatures for $\mathrm{ErFe}_{0.5}\mathrm{Cr}_{0.5}\mathrm{O}_3$ have been included, together with their corresponding calculated patterns, in Fig. 1. At the onset of magnetic order, near room temperature, a $\mathbf{G_x}$ structure belonging to the Γ_4 representation is adopted in all cases [Fig. 2(b)]. It is known that rare earth orthoferrites adopt this structure below T_{N1} [1]. On the other hand, some orthochromites, including TbCrO_3, DyCrO_3, and HoCrO_3, exhibit a different magnetic structure below their T_{N1}, i.e., a $\mathbf{G_z}$ ordering, consistent with the Γ_2 representation [Fig. 2(d)]. It follows that the $\mathbf{G_x}$ order is most likely due to the Fe^{3+}-O^{2-}-Fe^{3+} exchange interactions. The appearance of the $\mathbf{G_x}$ magnetic structure occurs at lower temperatures than in pure $R\mathrm{FeO}_3$ because of a dilution effect of Cr^{3+} ions. It is important to notice that a ferromagnetic **F** component along the c axis and an **A**-type antiferromagnetic arrangement along the b axis are allowed by symmetry within the same irreducible representation, but the M_y and M_z components were found to be close to zero or below the limit of detection during the initial refinement attempts, and were consequently fixed to zero during subsequent refinements.

As the temperature is lowered, the perovskites undergo a SR transition to a $\mathbf{G_z}$ ordering (Γ_2) in all cases. This occurs at different temperatures for each sample. The transition is not abrupt, occurring continuously within a finite temperature range in which the spin structure has two different **G** components. $\mathbf{G_x}$, $\mathbf{G_xG_z}$, and $\mathbf{G_z}$ structures are shown in Figs. 2(b), 2(c), and 2(d), respectively. This type of continuous rotational SR is caused by an increase in the polarization of the rare earth ions, which increases their effective anisotropy over the $\mathrm{Fe}^{3+}/\mathrm{Cr}^{3+}$ ions. The antisymmetric Dzyaloshinskii-Moriya and the anisotropic-symmetric exchange interactions produce an effective field for the $\mathrm{Fe}^{3+}/\mathrm{Cr}^{3+}$ ions. At lower

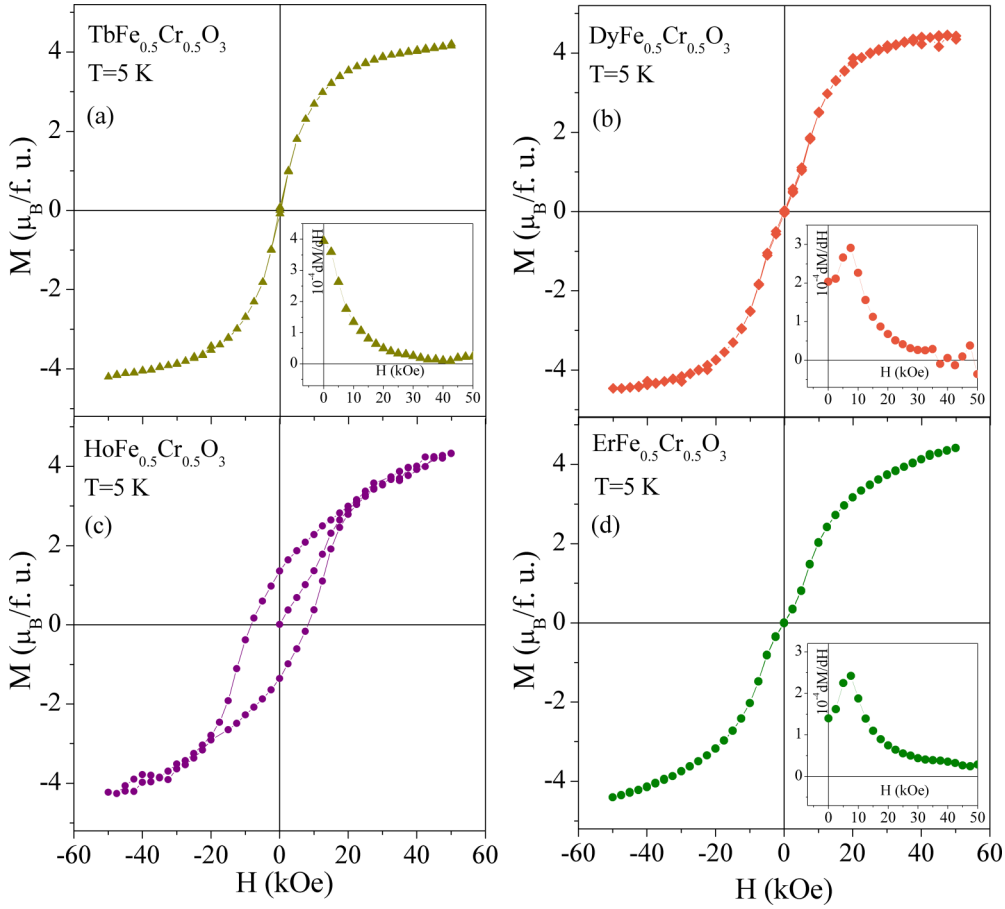

FIG. 4. Magnetization as a function of external magnetic field at 5 K for $R\mathrm{Fe}_{0.5}\mathrm{Cr}_{0.5}\mathrm{O}_3$ (R = Tb, Dy, Ho, and Er). Insets show dM/dH, displaying a characteristic break for $\mathrm{DyFe}_{0.5}\mathrm{Cr}_{0.5}\mathrm{O}_3$ and $\mathrm{ErFe}_{0.5}\mathrm{Cr}_{0.5}\mathrm{O}_3$ ascribed to a metamagnetic transition.

temperatures this effective field increases due to the increase of the R^{3+} magnetic moment polarization. The SR transition occurs when the absolute value of the interaction energy of Fe^{3+}/Cr^{3+} with the effective field exceeds that of the anisotropy energy of the M^{3+} ion. [7]. The presence of Cr^{3+} cations in the compounds adds complexity to this scenario because the strength of R^{3+}-Cr^{3+} coupling is higher than R^{3+}-Fe^{3+} coupling [2]. This will be reflected in the SR transition temperatures. These effects and the low temperature magnetic structures will be discussed separately for each sample in the following sections.

C. $\mathrm{TbFe}_{0.5}\mathrm{Cr}_{0.5}\mathrm{O}_3$

The first $\mathbf{G_x}$ to $\mathbf{G_z}$ SR for this sample takes place between ≈180 and 125 K. It is interesting to note that the Néel temperature for $TbCrO_3$, which adopts the same $\mathbf{G_z}$ ordering [31], is higher (167 K). $TbFeO_3$ eventually adopts this configuration too, but at much lower temperatures, close to 8 K [32,33]. It is clear that the Cr^{3+}-Tb^{3+} interaction is stronger than the Fe^{3+}-Tb^{3+} interaction, having a profound effect on the reorientation temperature. The refined magnetic moments, the magnetization curves, and the proposed magnetic configurations are shown in Fig. 5. In this figure, literature data for the magnetic structures as a function of temperature for the parent compounds $TbFeO_3$ and $TbCrO_3$ is schematically shown at the bottom of Fig. 5 [1,2,4,33].

The magnetic structure remains mostly invariant down to 15 K, where the ordering of the Tb^{3+} sublattice becomes evident. The magnetic structure of the transition metal sublattice is still consistent with the Γ_2 representation, displaying an $\mathbf{F_xC_y}$ ordering for Tb^{3+} ions [Figs. 5(b) and 6]. The maximum of net magnetization is also reached at this temperature. It is likely that the increase in magnetization while lowering the temperature down to this point is mainly due to the paramagnetic moments of Tb^{3+}. Below 15 K, the configuration of Tb^{3+} sublattice displays a net ferromagnetic component along the a axis. This type of ordering is also adopted by $TbCrO_3$ at approximately 4 K [36] and by $TbFeO_3$ between 3 and 8.5 K [33]. The same magnetic structure is conserved down to ≈8 K, where a new SR occurs in a narrow temperature range. The intermediate structure during this SR was solved from the NPD data and is sketched in Fig. 6. Below 8 K, the Fe^{3+}/Cr^{3+} moments revert to the high-temperature $\mathbf{G_x}$ ordering. This type of re-entrant SR transition, consisting of the return to a state compatible with the Γ_4 representation, has also been observed for $TbFeO_3$. When both sublattices are ordered in a manner compatible with Γ_2 it is likely that there exists some degree of coupling between Fe^{3+}/Cr^{3+} and Tb^{3+}. Below a certain temperature, these sublattices become decoupled, causing the return to a configuration belonging to Γ_4. It has been suggested that this decoupling is due to an increase in the dipolar interaction between Tb^{3+} cations

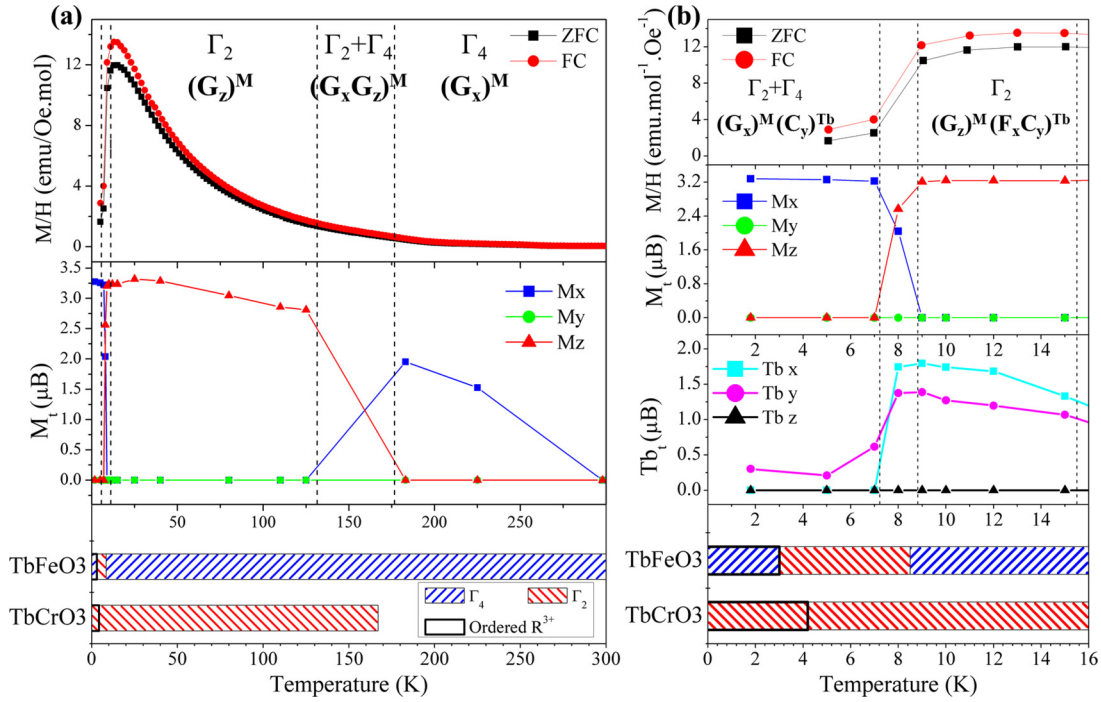

FIG. 5. (a) Magnetization and magnetic moment components obtained from NPD as a function of temperature for $TbFe_{0.5}Cr_{0.5}O_3$. (b) Zoom of the low temperature region. Lower panel corresponds to magnetic structure as a function of temperature for $TbFeO_3$ and $TbCrO_3$ obtained from literature [1,2,4,33].

at low temperatures [32]. The refined magnetic structure for $TbFe_{0.5}Cr_{0.5}O_3$ at low temperature is shown in Fig. 6.

A puzzling observation in this low temperature region is the fact that the Tb^{3+} magnetic moment components seem to drop abruptly with the SR transition at 8 K, with its ferromagnetic component ($\mathbf{F_x}$) becoming zero. At 1.9 K, only a small $\mathbf{C_y}$ component remains. This is accompanied by the appearance of diffuse scattering features in the low 2θ region of the NPD patterns, as seen in diffraction patterns for 1.9 and 25 K shown in Fig. 7. These features are indicated by two vertical arrows. Similar features have been previously reported in $TbCrO_3$, ascribed to short range magnetic interactions in the vicinity of a magnetic transition into a structure with a doubled unit cell. The remaining $\mathbf{C_y}$ component is explained by weak remains of the Tb^{3+}-Cr^{3+} coupling [36]. Broad features in the diffraction pattern have also been observed in NPD patterns for orthorhombic $TbFe_{0.5}Mn_{0.5}O_3$ in the 2θ region immediately below the 011 reflection, becoming more important at low temperatures. In that case, the authors proposed that this feature is related to spin fluctuations in the Tb^{3+} sublattice. Interestingly, this compound also shows a

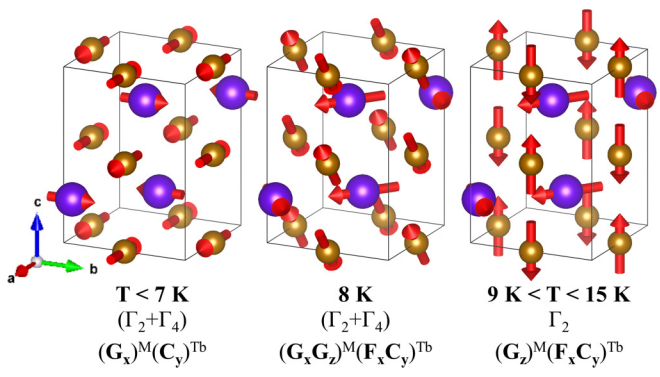

FIG. 6. Different magnetic structures of $TbFe_{0.5}Cr_{0.5}O_3$. Tb^{3+} ions are shown as blue spheres, Fe^{3+}/Cr^{3+} cations as brown spheres. O^{2-} anions are omitted for clarity. Magnetic moments are not scaled between temperatures. Tb^{3+} magnetic moment at $T < 7$ K has been multiplied by 3 to improve its visualization.

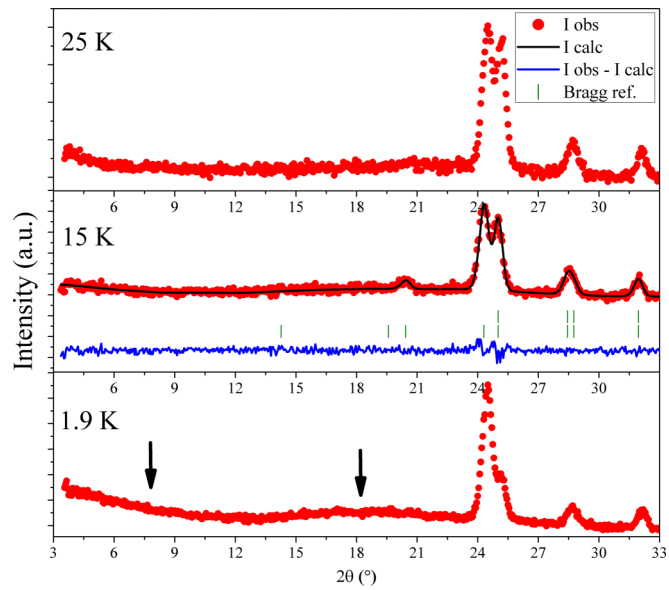

FIG. 7. NPD patterns for $TbFe_{0.5}Cr_{0.5}O_3$ at 1.9, 15, and 25 K. Two wide features appear in the low angle region at the lowest temperature, indicated with arrows.

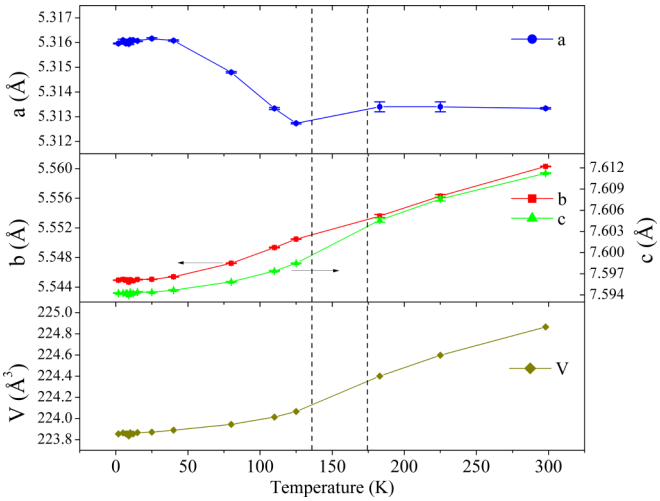

FIG. 8. Cell parameters and cell volume of $TbFe_{0.5}Cr_{0.5}O_3$ as a function of temperature. Dashed lines mark the temperature range of the $\mathbf{G_x}$-$\mathbf{G_z}$ (Γ_4 to Γ_2) spin reorientation transition.

re-entrant SR transition [37]. These short range interactions in Tb^{3+} are likely antiferromagnetic in nature, which would explain the magnetization drop after abandoning the previous $\mathbf{F_xC_y}$ ordering that allowed a net ferromagnetic moment. This short range order of Tb^{3+} is also a probable cause for the disappearance of most of the Tb^{3+}-M^{3+} coupling [38].

This perovskite displays another interesting property. Usually, as temperature lowers, cell parameters also decrease. In the case of $TbFe_{0.5}Cr_{0.5}O_3$ this does not apply completely. As shown in Fig. 8, the *a* parameter markedly increases below 125 K. The increase goes up to 0.065%. This occurs simultaneously with the magnetic ordering of the transition metal sublattice into the $\mathbf{G_z}$ mode, belonging to Γ_2. Similar observations have been made for $YbFe_{0.5}Cr_{0.5}O_3$ (0.06% in volume) and $TmFe_{0.5}Cr_{0.5}O_3$ (0.04% for *a* axis) [14]. The linkage between the onset of the expansion and the spin reorientation strongly points at a magnetic origin for the change in size. It has been suggested that this effect is due to a magnetoelastic effect produced by the repulsion between magnetic moments of neighboring transition metal ions [14]. This effect was not observed in any other of the perovskites presented in this study.

D. $HoFe_{0.5}Cr_{0.5}O_3$

The magnetization and the individual magnetic moment components refined from NPD data for this sample are displayed in Fig. 9, together with literature data for the magnetic structures of $HoFeO_3$ and $HoCrO_3$ schematically shown at the bottom of Fig. 9 [1,2,4]. The first SR for this compound begins between 200 and 180 K, ending around 130 K. As in the case of $TbFe_{0.5}Cr_{0.5}O_3$, this transition temperature range matches the antiferromagnetic ordering temperature of $HoCrO_3$, which also orders in a $\mathbf{G_z}$ structure [2], hinting at the importance of Cr^{3+} interactions. The transition temperature also matches with a report on very similar $HoFe_{1-x}Cr_xO_3$ compounds, being higher than in $HoFe_{0.6}Cr_{0.4}O_3$ but lower than in $HoFe_{0.4}Cr_{0.6}O_3$ [39]. The trend confirms that Cr^{3+}-Ho^{3+} interactions are more prominent than Fe^{3+}-Ho^{3+}

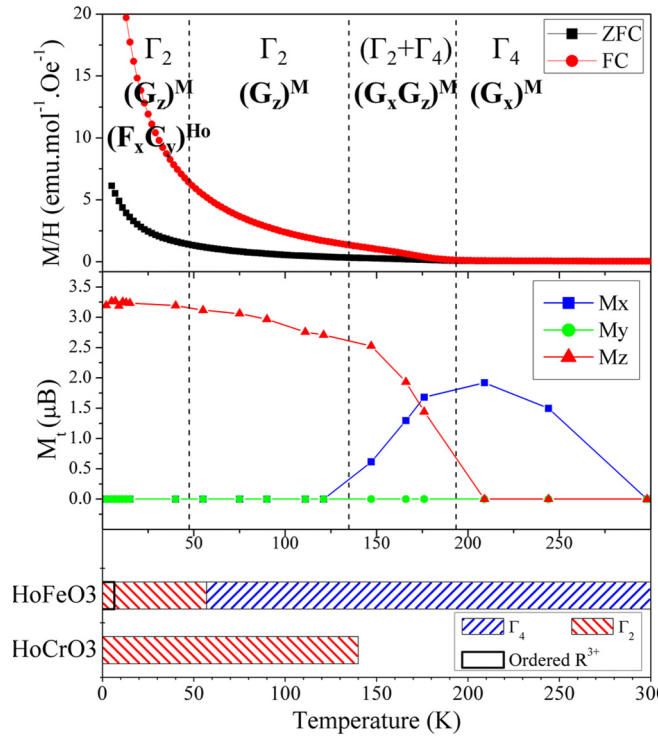

FIG. 9. Magnetization and magnetic moment components obtained from NPD for $HoFe_{0.5}Cr_{0.5}O_3$. Lower panel corresponds to magnetic structures as a function of temperature for $HoFeO_3$ and $HoCrO_3$ obtained from literature [1,2,4].

interactions, as an increase in Cr^{3+} content produces an increase on the SR temperature.

At 45 K Ho^{3+} ions are found to be ordered with an $\mathbf{F_xC_y}$ mode, also belonging to the Γ_2 representation. The configuration of this ordering is equivalent to the one found for $TbFe_{0.5}Cr_{0.5}O_3$ between 8 and 15 K. This ordering of Ho^{3+} has also been noticed recently at 35 K in the similar compound $HoFe_{0.4}Cr_{0.6}O_3$ [39]. No changes in the magnetic structure were observed with further decrease of temperature down to 1.9 K except for the continuous increase of the magnetic moment for Ho^{3+} ions.

E. $ErFe_{0.5}Cr_{0.5}O_3$

In the $ErFe_{0.5}Cr_{0.5}O_3$ magnetization measurement there is a visible change on the slope at approximately 160 K (see Figs. 3 and 10). This is very close to the temperature observed as the onset of the first SR transition in the NPD measurement, as shown in Fig. 10. Literature data for the magnetic structures for the parent compounds $ErFeO_3$ and $ErCrO_3$ is schematically shown at the bottom of Fig. 10 [1,2,4,34,35]. The $\mathbf{G_x}$ to $\mathbf{G_z}$ SR transition is observed in $ErFeO_3$ close to 100 K [35]. This transition is continuous in nature, but a two-step transition under an oscillating magnetic field has been reported, suggesting a more complex magnetic structure [40]. The increase in the SR temperature in our $ErFe_{0.5}Cr_{0.5}O_3$ sample compared to $ErFeO_3$, also suggests that Cr^{3+}-Er^{3+} interactions are more prominent than Fe^{3+}-Er^{3+} interactions.

The $\mathbf{G_z}$ configuration for the Fe^{3+}/Cr^{3+} sublattice remains invariant down to 9 K, where a $\mathbf{C_z}$ component (from

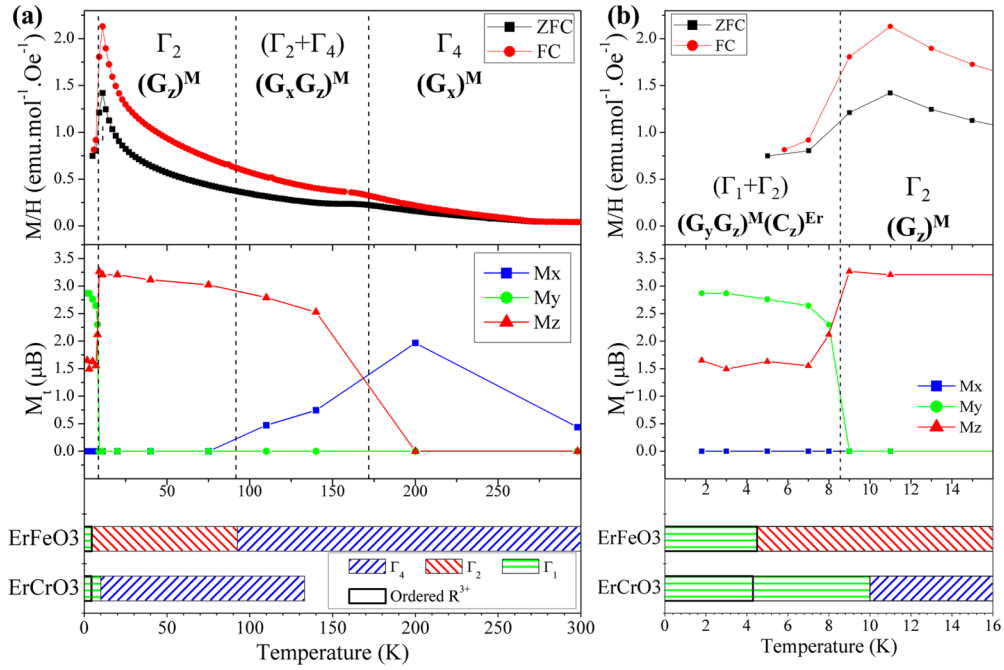

FIG. 10. (a) Magnetization and magnetic moment components obtained from NPD for $ErFe_{0.5}Cr_{0.5}O_3$. (b) Zoom of the low temperature region. Lower panel corresponds to magnetic structure as a function of temperature for $ErFeO_3$ and $ErCrO_3$ obtained from literature [1,2,4,34,35].

representation Γ_1) appears on the Er^{3+} sublattice. Very close to this temperature, at 8 K, a second SR transition takes place on the Fe^{3+}/Cr^{3+} sublattice: a $\mathbf{G_y}$ component appears, also belonging to Γ_1. This has been assigned as an "incomplete" transition, since the final structure at 1.9 K still includes both $\mathbf{G_y}$ and $\mathbf{G_z}$ components. The observed sequence of magnetic structures in this reorientation is illustrated in Fig. 11. All these processes happen in a rather narrow temperature range of about 2 K while displaying a sudden drop in the magnetization. This drop could be explained by the ordering of the paramagnetic Er^{3+} ions into an antiferromagnetic structure $\mathbf{C_z}$. This specific sequence of ordering and reorientation has been reported previously for $ErFeO_3$ in the vicinity of 4.5 K [41]. A $\mathbf{G_z}$ to $\mathbf{G_y}$ transition has also been reported for $ErCrO_3$ close to 9 K, accompanied by disappearance of magnetization [42]. Both reports agree on the abrupt nature of the transition. The mechanisms and exchanges that produce these rotations

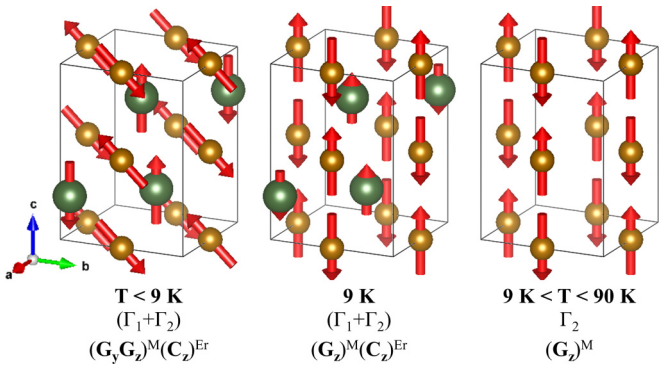

FIG. 11. Different magnetic structures of $ErFe_{0.5}Cr_{0.5}O_3$ at low temperatures. Er^{3+} ions are shown as green spheres, Fe^{3+}/Cr^{3+} cations as brown spheres. O^{2-} anions are omitted for clarity.

are not completely clear, but it is probable that the Er^{3+} sublattice becomes cooperatively ordered, inducing rotation on the Fe^{3+}/Cr^{3+} sublattice. All explanations are in agreement with an increase in the strength of the (Fe^{3+}/Cr^{3+})-Er^{3+} interaction at low temperatures.

F. Discussing $DyFe_{0.5}Cr_{0.5}O_3$ as a combination of $DyFeO_3$ and $DyCrO_3$

Taking into account the observations made in the compounds discussed above it is likely that at least some of the transitions of $DyFe_{0.5}Cr_{0.5}O_3$ can be predicted from a combination of the transitions observed in $DyFeO_3$ and $DyCrO_3$, albeit with some temperature shifts. $DyFeO_3$ orders antiferromagnetically in a $\mathbf{G_x}$ configuration (Γ_4) below 650 K, and presents a SR transition to a $\mathbf{G_y}$ configuration (Γ_1) at approximately 36 K [43]. The Dy^{3+} sublattice shows ordering below 3.7 K [44]. Meanwhile, $DyCrO_3$ orders in a $\mathbf{G_z}$ configuration (Γ_2) below 147 K and presents no SR. In this last case, the Dy^{3+} sublattice orders at 2.1 K [4]. We could therefore infer that a continuous SR transition from $\mathbf{G_x}$ to $\mathbf{G_z}$ configuration might take place at a temperature close to 147 K, with an additional SR transition from $\mathbf{G_z}$ to $\mathbf{G_y}$ configuration occurring at a lower temperature, below 36 K.

This is similar to what is observed in our NPD measurements for $DyFe_{0.5}Cr_{0.5}O_3$. The refined magnetic moments and the magnetization measurements as a function of temperature are shown in Fig. 12. Literature data for the magnetic structures for the parent compounds $DyFeO_3$ and $DyCrO_3$ is schematically shown at the bottom of Fig. 12 [1,2,4,15]. The high temperature magnetic order belongs to the $\mathbf{G_x}$ configuration (Γ_4), until the first SR transition to $\mathbf{G_z}$ (Γ_2) takes place between ≈125 and ≈65 K. In this range, the system shows a mixed $\mathbf{G_xG_z}$ configuration, as observed in

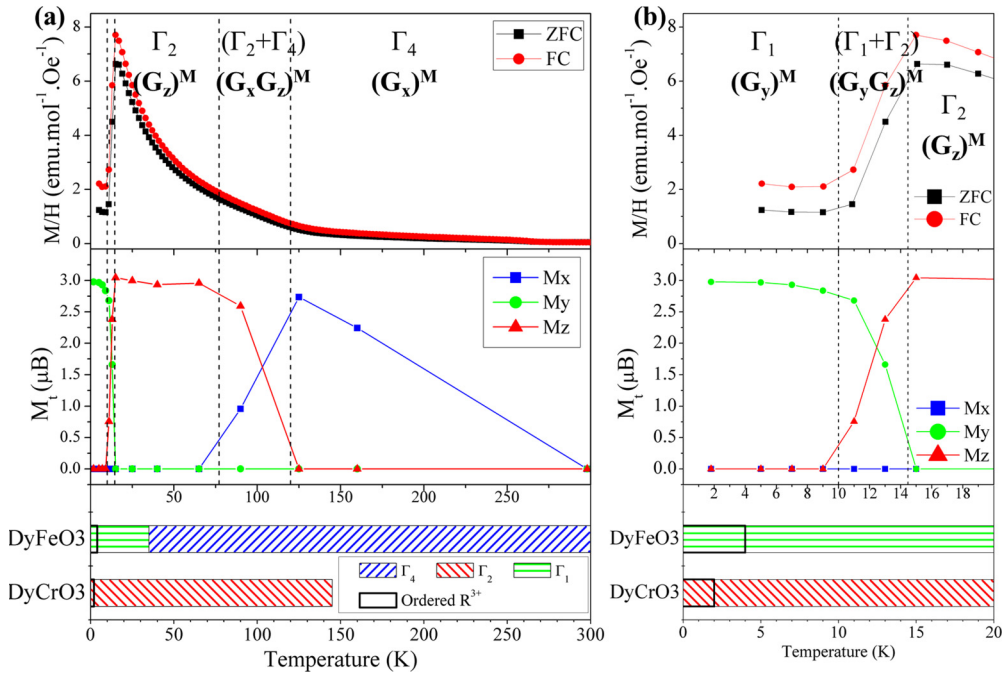

FIG. 12. (a) Magnetization and magnetic moment components obtained from NPD as a function of temperature for $DyFe_{0.5}Cr_{0.5}O_3$. (b) Zoom of the low temperature region. Lower panel corresponds to magnetic structure as a function of temperature for $DyFeO_3$ and $DyCrO_3$ obtained from literature [1,2,4,15].

$ErFe_{0.5}Cr_{0.5}O_3$. Below ≈65 K the configuration is completely $\mathbf{G_z}$, belonging to the Γ_2 representation. The second SR takes place between ≈15 and ≈8 K, moving onto a $\mathbf{G_y}$ ordering (Γ_1). In between these temperatures a mixed $\mathbf{G_yG_z}$ ordering is observed. Finally, below 8 K the magnetic structure reaches a $\mathbf{G_y}$ order. There is no evidence on any type of long range ordering in the Dy^{3+} sublattice at the measured temperatures.

The good agreement between the sequence of transitions inferred from $DyFeO_3$ and $DyCrO_3$ properties and the experimental results proves a certain predictive capacity of this method. Thus, the final magnetic properties of the mixed orthochromite-orthoferrite systems are tightly connected to their Fe-only or Cr-only counterparts.

G. Metamagnetism in $ErFe_{0.5}Cr_{0.5}O_3$ and $DyFe_{0.5}Cr_{0.5}O_3$

Erbium and dysprosium perovskites display a metamagnetic (MM) behavior in their isothermal magnetization measurements at 5 K (see Fig. 4). It must be emphasized that these are the two systems in which the Fe^{3+}/Cr^{3+} sublattice displays a $\mathbf{G_y}$ ordering (Γ_1) at this temperature. As a means to assess the connection between these phenomena, additional isothermal magnetization measurements were performed for these samples. The results of these measurements for $DyFe_{0.5}Cr_{0.5}O_3$ are shown in Fig. 13. The transition field value for the MM transition is arbitrarily taken as that displaying the maximum in dM/dH. The MM transition is observed in the $5 \leqslant T \leqslant 12$ K temperature range for H values between 4 and 7 kOe. This is in perfect agreement with the temperature at which the Γ_1 configuration is completed for this compound [see Fig. 12(b)]. The MM transition becomes smoother as the temperature increases. Above 13 K this transition is suppressed, i.e., at the end of the $\Gamma_1 \rightarrow \Gamma_2$ transition [see Fig. 12(b)]. $ErFe_{0.5}Cr_{0.5}O_3$ which also shows the MM behavior below 9 K presents a SR transition between the Γ_1 and Γ_2 configurations below that temperature (see Fig. 10(b) and Fig. SM-1 in the Supplemental Material [29]). This

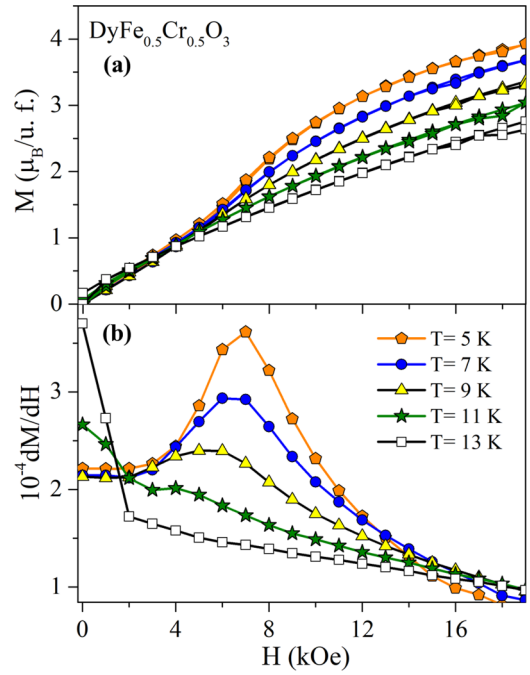

FIG. 13. (a) M and (b) dM/dH as a function of temperature for $DyFe_{0.5}Cr_{0.5}O_3$. The external magnetic field for the metamagnetic transition occurring in the temperature range $5 \leqslant T \leqslant 12$ K is taken at the maximum of dM/dH.

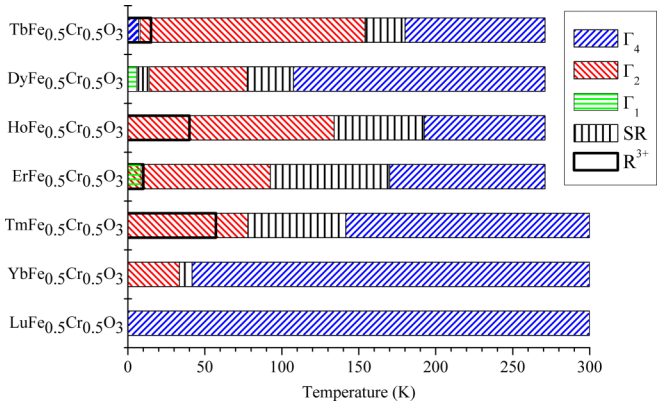

FIG. 14. Magnetic phase diagram for $R\mathrm{Fe}_{0.5}\mathrm{Cr}_{0.5}\mathrm{O}_3$ (R = Tb, Dy, Ho, Er, Tm, Yb, and Lu). Results for Tm, Yb, and Lu obtained from Pomiro *et al.* [14]. A detail of the low temperature region is included in Fig. SM-2.

further supports the relationship between the MM transition and the Γ_1 configuration.

The MM transition is proposed to occur when the exchange field (H_m) or the anisotropy field (H_a) acting on the magnetic moments is comparable to the applied external field [45]. In general the MM transition in rare earth complex oxides has been assigned to the field-induced destruction of the antiferromagnetic order of the rare earth sublattice [46]. This last explanation is not valid in our case since the MM transition is observed in $\mathrm{DyFe}_{0.5}\mathrm{Cr}_{0.5}\mathrm{O}_3$ in which Dy^{3+} is not ordered at least down to 1.9 K. Moreover, for $\mathrm{HoFe}_{0.5}\mathrm{Cr}_{0.5}\mathrm{O}_3$, although Ho^{3+} is ordered at ≈45 K, no MM transition is observed. Another possible explanation was attributed to the coexistence of two magnetic phases, i.e., AFM and FM, as in the case of (Pr, Ca, Sr)MnO_3 perovskites [47,48]. Again, this magnetic phase coexistence is not observed in our compounds.

The MM transition occurs in the temperature range where the Γ_1 phase exists, only for $\mathrm{DyFe}_{0.5}\mathrm{Cr}_{0.5}\mathrm{O}_3$ and $\mathrm{ErFe}_{0.5}\mathrm{Cr}_{0.5}\mathrm{O}_3$. As the $\Gamma_2 \rightarrow \Gamma_1$ reorientation is observed by NPD only at very low temperature (≈9 K), it suggests that those magnetic orderings possess very similar energies. Accordingly, we suggest that the application of the external magnetic field H in the temperature region where Γ_1 exists might induce a switching of the magnetic ordering from Γ_1 to Γ_2. However, NPD experiments under applied magnetic field are necessary to confirm this hypothesis.

IV. CONCLUDING REMARKS

Based on the present results, we have been able to build a complete magnetic phase diagram for the $R\mathrm{Fe}_{0.5}\mathrm{Cr}_{0.5}\mathrm{O}_3$ compounds with details of the transition metal sublattice SR transitions and the R^{3+} sublattice ordering by means of magnetization measurements (as a function of temperature and applied field) and NPD experiments in the temperature range 1.9–300 K (Fig. 14, with a low temperature detail in Fig. SM-2 in the Supplemental Material [29]). All compounds present a high temperature Γ_4 magnetic phase for the transition metal sublattice. For all the compounds a second order transition $\Gamma_4 \rightarrow (\Gamma_4 + \Gamma_2) \rightarrow \Gamma_2$ [5] is observed in a more or less broad temperature range, with the exception of Lu^{3+}, i.e., a diamagnetic R^{3+} cation. At first, it may seem that the presence of a paramagnetic R^{3+} is necessary condition for the appearance of a SR transition. However, it is important to note that this is not always the case. Some $R\mathrm{MO}_3$ perovskites with paramagnetic R^{3+} cations do not display a spin reorientation transition, e.g., GdFeO_3 and TbCrO_3 [12,31]. As it was mentioned before, there are also cases where R^{3+} is diamagnetic, but the SR transition is caused by the magnetic anisotropy contribution of an M^{3+} cation, e.g., Mn^{3+} in $\mathrm{YFe}_{1-x}\mathrm{Mn}_x\mathrm{O}_3$ [8].This highlights the uniqueness of each R^{3+}-M^{3+} exchange interaction, and shows how mixtures of multiple cations will result in even more complex magnetic behaviors.

Below this transition temperature, the behavior is highly dependent on the rare earth cation. At the temperature range of the $\Gamma_4 \rightarrow \Gamma_2$ SR all rare earth cations are in a paramagnetic state, but they feel the internal magnetic field created by the $\mathrm{Fe}^{3+}/\mathrm{Cr}^{3+}$ sublattice which tends to partially order them [1]. $\mathrm{HoFe}_{0.5}\mathrm{Cr}_{0.5}\mathrm{O}_3$ does not show any other SR transition down to 1.9 K but shows Ho^{3+} sublattice ordering at a relatively high temperature (45 K). $\mathrm{DyFe}_{0.5}\mathrm{Cr}_{0.5}\mathrm{O}_3$ and $\mathrm{ErFe}_{0.5}\mathrm{Cr}_{0.5}\mathrm{O}_3$ exhibit a second SR transition in their transition metal sublattice, from Γ_2 to Γ_1 at very low temperatures (15 and 8 K, respectively). For the Er compound the transition is incomplete, displaying a magnetic structure compatible with a combination of Γ_2 and Γ_1 even at 1.9 K. For these two compounds a metamagnetic transition is observed for an external magnetic field of $H \approx 7$ kOe. The fact that this is only observed for the compounds showing the second SR from $\Gamma_2 \rightarrow \Gamma_1$, and around the transition temperature, suggests that a correlation exists between this SR transition and the MM transition. We propose that the external magnetic field might induce a transition $\Gamma_1 \rightarrow \Gamma_2$. The latter cannot be simply ascribed to the R^{3+} magnetic ordering since the Dy^{3+} sublattice does not display long-range order at any temperature down to 1.9 K, while the Er^{3+} sublattice orders at 8.5 K.

$\mathrm{TbFe}_{0.5}\mathrm{Cr}_{0.5}\mathrm{O}_3$ is the only member that shows a re-entrant SR to Γ_4 at very low temperatures. This type of re-entrant SR transition consists of the return to a state compatible with the Γ_4 representation. When both sublattices are ordered within Γ_2 it is likely that there exists some degree of coupling between $\mathrm{Fe}^{3+}/\mathrm{Cr}^{3+}$ and Tb^{3+}. Below a certain temperature, these sublattices become decoupled as evidenced by the return to a configuration belonging to Γ_4. It has been suggested that this decoupling is due to an increase in the dipolar interaction between Tb^{3+} cations at low temperatures [32].

Finally, our study allows us to propose a methodology. The spin reorientation transition temperature and the type of magnetic ordering can be qualitatively predicted for the $R\mathrm{Fe}_{0.5}\mathrm{Cr}_{0.5}\mathrm{O}_3$ series based on the observed results for the pure compounds $R\mathrm{FeO}_3$ and $R\mathrm{CrO}_3$.

ACKNOWLEDGMENTS

R.E.C. wants to thank CONICET, PIP No. 11220120100360, the Agencia Nacional de Promoción Científica y Tecnológica (ANPCyT), PICT No. 2016–2495, and the Secretaría de Ciencia y Tecnología de la Universidad Nacional de Córdoba (SECyT-UNC), Project No. 113/17 for financial support. R.D.S. and G.A. acknowledge financial support from the ANPCyT, PICT No. 2017-705 and the

Secretaría de Ciencia y Tecnología de la Universidad Nacional de Cuyo (SECyT-UNCuyo), Project No. 06/C519. R.E.C. and G.A. acknowledge financial support from a Seed Money Grant 2015–2016 by the EPFL Leading House—Swiss Bilateral Programmes. We gratefully acknowledge Paul Scherrer Institute PSI (Villigen, Switzerland) for access to neutron powder diffraction instruments and the excellent support received during our stay. The work was partially performed at the Swiss Spallation Neutron Source SINQ (PSI). F.P. and J.P.B. thank CONICET for their fellowships.

[1] R. L. White, J. Appl. Phys. **40**, 1061 (1969).
[2] R. M. Hornreich, J. Magn. Magn. Mater. **7**, 280 (1978).
[3] D. Treves, J. Appl. Phys. **36**, 1033 (1965).
[4] E. F. Bertaut, J. Mareschal, G. De Vries, R. Aléonard, R. Pauthenet, J. P. Rebouillat, and V. Zarubicka, IEEE Trans. Magn. **2**, 453 (1966).
[5] Ya. B. Bazaliy, L. T. Tsymbal, G. N. Kakazei, A. I. Izotov, and P. E. Wigen, Phys. Rev. B **69**, 104429 (2004).
[6] A. V. Kimel, A. Kirilyuk, A. Tsvetkov, R. V. Pisarev, and Th. Rasing, Nature (London) **429**, 850 (2004).
[7] T. Yamaguchi, J. Phys. Chem. Solids **35**, 479 (1974).
[8] P. Mandal, C. R. Serrao, E. Suard, V. Caignaert, B. Raveau, A. Sundaresan, and C. N. R. Rao, J. Solid State Chem. **197**, 408 (2013).
[9] S. Yin, V. Sharma, A. McDannald, F. A. Reboredo, and M. Jain, RSC Adv. **6**, 9475 (2016).
[10] L. H. Yin, J. Yang, P. Tong, X. Luo, W. H. Song, J. M. Dai, X. B. Zhu, and Y. P. Sun, Appl. Phys. Lett. **110**, 192904 (2017).
[11] L. H. Yin, J. Yang, P. Tong, X. Luo, C. B. Park, K. W. Shin, W. Song, J. Dai, K. H. Kim, X. Zhu, and Y. Sun, J. Mater. Chem. C **4**, 11198 (2016).
[12] M. Das, S. Roy, and P. Mandal, Phys. Rev. B **96**, 174405 (2017).
[13] O. V. Billoni, F. Pomiro, S. A. Cannas, C. Martin, A. Maignan, and R. E. Carbonio, J. Phys.: Condens. Matter **28**, 476003 (2016).
[14] F. Pomiro, R. D. Sánchez, G. Cuello, A. Maignan, C. Martin, and R. E. Carbonio, Phys. Rev. B **94**, 134402 (2016).
[15] V. G. Nair, L. Pal, V. Subramanian, and P. N. Santhosh, J. Appl. Phys. **115**, 17D728 (2014).
[16] G. Kotnana and S. Narayana Jammalamadaka, J. Magn. Magn. Mater. **418**, 81 (2016).
[17] N. Ramu, R. Muralidharan, K. Meera, and Y. H. Jeong, RSC Adv. **6**, 72295 (2016).
[18] K. R. S. Preethi Meher, A. Wahl, A. Maignan, C. Martin, and O. I. Lebedev, Phys. Rev. B **89**, 144401 (2014).
[19] J. H. Lee, Y. K. Jeong, J. H. Park, M. A. Oak, H. M. Jang, J. Y. Son, and J. F. Scott, Phys. Rev. Lett. **107**, 117201 (2011).
[20] B. Rajeswaran, P. Mandal, R. Saha, E. Suard, A. Sundaresan, and C. N. R. Rao, Chem. Mater. **24**, 3591 (2012).
[21] B. Rajeswaran, D. I. Khomskii, A. K. Zvezdin, C. N. R. Rao, and A. Sundaresan, Phys. Rev. B **86**, 214409 (2012).
[22] B. Rajeswaran, D. Sanyal, M. Chakrabarti, Y. Sundarayya, A. Sundaresan, and C. N. R. Rao, Europhys. Lett. **101**, 17001 (2013).
[23] D. Singh, S. Gupta, and A. Mahajan, Ceram. Int. **42**, 11020 (2016).
[24] P. Tirupathi, P. Justin, K. Prabahar, and M. Poster, J. Alloys Compd. **731**, 411 (2017).
[25] M. Xiang, Y. Cao, W. Zhao, B. Kang, Z. Feng, P. Sharma, J. Zhang, W. Ren, and S. Cao, J. Supercond. Nov. Magn. **30**, 2791 (2017).
[26] H. M. Rietveld, J. Appl. Crystallogr. **2**, 65 (1969).
[27] J. Rodríguez-Carvajal, Physica B **192**, 55 (1993).
[28] K. Momma and F. Izumi, J. Appl. Crystallogr. **44**, 1272 (2011).
[29] See Supplemental Material at http://link.aps.org/supplemental/10.1103/PhysRevB.98.134417 for (Table SM-I) additional information from Rietveld refinement of NPD data, (Fig. SM-1) $M(H)$ and dM/dH for $ErFe_{0.5}Cr_{0.5}O_3$, and (Fig. SM-2) a detail of the low temperature region of Fig. 14.
[30] E. F. Bertaut, Acta Crystallogr. Sect. A **24**, 217 (1968).
[31] J. D. Gordon, R. M. Hornreich, and S. Shtrikman, Phys. Rev. B **13**, 3012 (1976).
[32] E. F. Bertaut, J. Chappert, J. Mareschal, J. P. Rebouillat, and J. Sivardière, Solid State Commun. **5**, 293 (1967).
[33] S. Artyukhin, M. Mostovoy, N. Paduraru Jensen, D. Le, K. Prokes, V. G. de Paula, H. N. Bordallo, A. Maljuk, S. Landsgesell, H. Ryll *et al.*, Nat. Mater. **11**, 694 (2012).
[34] Y. Su, J. Zhang, L. Li, B. Li, Y. Zhou, D. Deng, Z. Chen, and S. Cao, Appl. Phys. A **100**, 73 (2010).
[35] G. Deng, P. Guo, W. Ren, S. Cao, H. E. Maynard-Casely, M. Adveev, and G. J. McIntyre, J. Appl. Phys. **117**, 164105 (2015).
[36] E. F. Bertaut, J. Mareschal, and G. F. de Vries, J. Phys. Chem. Solids **28**, 2143 (1967).
[37] H. S. Nair, T. Chatterji, C. M. N. Kumar, T. Hansen, H. Nhalil, S. Elizabeth, and A. M. Strydom, J. App. Phys. **119**, 053901 (2016).
[38] J. Mareschal, J. Sivardière, G. F. de Vries, and E. F. Bertaut, J. Appl. Phys. **39**, 1364 (1968).
[39] X. Liu, L. Hao, Y. Liu, X. Ma, S. Meng, Y. Li, J. Gao, H. Guo, W. Han, K. Sun *et al.*, J. Magn. Magn. Mater. **417**, 382 (2016).
[40] H. Shen, Z. Chang, F. Hong, J. Xu, S. Yuan, S. Cao and X. Wang, Appl. Phys. Lett. **103**, 192404 (2013).
[41] G. Gorodetsky, R. M. Hornreich, I. Yaeger, H. Pinto, G. Shachar and H. Shaked, Phys. Rev. B **8**, 3398 (1973).
[42] M. Eibschutz, L. Holmes, J. P. Malta, and L. G. Van Uitert, Solid State Commun. **8**, 1815 (1970).
[43] G. Gorodetsky, B. Sharon, and S. Shtrikman, J. Appl. Phys. **39**, 1371 (1968).
[44] A. Berton and B. Sharon, J. Appl. Phys. **39**, 1367 (1968).
[45] T. Taniguchi, Y. Kawaji, T. C. Ozawa, Y. Nagata, Y. Noro, H. Samata, and M. D. Lan, J. Alloys Compd. **386**, 63 (2005).
[46] R. Z. Levitin, B. V. Mill, V. V. Moschalkov, N. A. Samarin, V. V. Snegirev, and Y. Zoubkova, Solid State Commun. **73**, 443 (1990).
[47] V. S. Kolat, T. Izgi, A. O. Kaya, N. Bayri, H. Gencer, and S. Atalay, J. Magn. Magn. Mater. **322**, 427 (2010).
[48] S. Hébert, A. Maignan, V. Hardy, C. Martin, M. Hervieu, B. Raveau, R. Mahendiran, and P. Schiffer, Eur. Phys. J. B **29**, 419 (2002).